materials

MDPI

Article

Hydrothermal Synthesis and Optical Properties of Magneto-Optical Na_3FeF_6:Tb^{3+} Octahedral Particles

Zhiguo Zhao [1,*,†] and Xue Li [2,*,†]

[1] Key Laboratory of Electromagnetic Transformation and Detection of Henan province, Luoyang Normal University, Luoyang 471934, China

[2] School of Materials Science and Engineering, Zhejiang Sci-Tech University, Xiasha University Town, Hangzhou 310018, China

* Correspondence: zhiguo.zhao@tom.com (Z.Z.); lixue5306@163.com (X.L.)

† Z.Z. and X.L. contributed equally.

Received: 13 December 2019; Accepted: 9 January 2020; Published: 10 January 2020

Abstract: Sodium iron hexafluoride (Na_3FeF_6), as a colorless iron fluoride, is expected to be an ideal host for rare earth ions to realize magneto-optical bi-functionality. Herein, monodispersed terbium ions (Tb^{3+}) doped Na_3FeF_6 particles are successfully synthesized by a facile one-pot hydrothermal process. X-ray diffraction (XRD) and Field emission scanning electron microscopy (FESEM) reveal that the Tb^{3+} doped Na_3FeF_6 micro-particles with regular octahedral shape can be assigned to a monoclinic crystal structure (space group P21/c). Under ultraviolet light excitation, the Na_3FeF_6:Tb^{3+} octahedral particles given orange-red light emission originated from the $^5D_4 \rightarrow {}^7F_J$ transitions of the Tb^{3+} ions. In addition, the magnetism measurement indicates that Na_3FeF_6:Tb^{3+} octahedral particles are paramagnetic with high magnetization at room temperature. Therefore, the Na_3FeF_6:Tb^{3+} powders may find potential applications in the biomedical field as magnetic-optical bi-functional materials.

Keywords: magnetic-optical bi-functional materials; hydrothermal process; down-conversion luminescence; Na_3FeF_6:Tb^{3+}

1. Introduction

Bi-functional materials with distinct magnetic and fluorescent (luminescent) properties have received considerable attention [1,2] due to their potential applications in magnetic resonance imaging [3], targeted drug delivery [4], sensors [5,6], optical isolators [7–9], high accuracy communication [10], and aircraft guidance [11]. To date, there have been a few reports about the synthesis of magnetically-functionalized luminescent materials based on quantum dots (QDs) and organic dyes [12]. However, QDs features notorious disadvantages including chemical instability, potential toxicity, luminescent intermittence and weakly magnetic, while organic dyes typically exhibit rapid photobleaching and a low fluorescence quantum yield [13]. As a result, biological applications of these materials have been seriously restricted.

Rare-earth (RE) ions doped inorganic materials can be considered as alternative luminescent materials in which the above limitations are partly circumvented [14,15]. Nowadays, great efforts have been devoted to the design and fabrication of magneto-optical bi-functional systems based on RE-doped up-conversion or down-conversion materials, such as Gd_2O_3: Er^{3+}/Yb^{3+} [16], $GdPO_4$: Eu^{3+} [17], YVO_4: Er^{3+} [18], $Tb_{0.94}Pr_{0.06}VO_4$ [19] and $NaYF_4$: Yb, Ho [20]. However, studies of magneto-optical effects usually have to rely on materials with a high magnetic movement, which are usually non-transparent. On the other hand, the introduction of strong magnetic (ferromagnetic) materials can be achieved by fabricating magnetic-core/luminescent-shell structures, such as the Fe_3O_4@LaF_3:Yb^{3+}, Er^{3+} [21], Fe_3O_4@α-$NaYF_4$/Yb [13] and Fe_3O_4@ZnO:Er^{3+},Yb^{3+} [22]. However, the preparation processes for

core-shell structures is complicated, and more importantly, magnetic oxide, Fe_3O_4, strongly absorbs visible light and quenches fluorescence of the RE ions [23]. Therefore, use of a colorless, strongly magnetic host is of great importance for the development of magneto-optical bifunctional materials.

In this work, colorless Tb^{3+} ions doped sodium iron hexafluoride (Na_3FeF_6:Tb^{3+}) containing a high centration of paramagnetic ion (Fe^{3+}) is synthesized through a simple hydrothermal process. The Na_3FeF_6:Tb^{3+} particles give distinct visible emission under excitation by UV light and its luminescence intensity is optimized by adjusting Tb^{3+} doping concentration. The investigation of the magnetic property reveals that the Na_3FeF_6:Tb^{3+} particles are paramagnetic at room temperature. These results indicate that Na_3FeF_6:Tb^{3+} particles might be promising as a new platform for exploiting magnetic-optical functionalities.

2. Materials and Methods

2.1. Synthesis of Na_3FeF_6:Tb^{3+} Particles

The reagents used in this work were analytical-grade $Fe(NO_3)_3{\cdot}9H_2O$ (99.99%), NH_4HF_2 (99%), NaF (99%), HF (40%), and $Tb(NO_3)_3{\cdot}6H_2O$ (99.99%) (Xiya Reagent, Shandong, China). Samples with a different molar ratio of Tb^{3+} to Fe^{3+} (5%, 10%, 15%, 18%, and 20%) were synthesized by a hydrothermal method under the same conditions. Here, we take Na_3FeF_6:18%Tb^{3+} as an example to present the detailed preparation procedure. The process mainly involves four steps: (1) 14 mL of $Fe(NO_3)_3{\cdot}9H_2O$ solution (0.1 M), 14 mL of NaF solution (0.5 M), 42 mL of NH_4HF_2 solution (0.5 M), and 3 mL of HF were mixed under vigorous magnetic stirring for 30 min; (2) 2.7 mL $Tb(NO_3)_3{\cdot}6H_2O$ was added to the above solution under vigorous magnetic stirring for 3 h; (3) after stirring for 3 h, the above solution was transferred into a Teflon-lined stainless steel autoclave (capacity 100 mL), which was heated at 190 °C for 12 h and cooled naturally to room temperature; (4) the obtained sample was washed by deionized water for several times and dried at 60 °C overnight.

2.2. Characterization

Phase identification of the as-prepared samples were carried out by X-ray diffraction (XRD) (X'Pert Pro, PANalytical BV, Netherland) with Cu Kα radiation (λ = 1.5418 Å). The microstructure and element mapping of particles were observed with a Field emission scanning electron microscopy (FESEM) (Hitachi Ltd., Tokyo, Japan) equipped with an energy dispersive spectroscopy (EDS). UV-Vis (ultraviolet-visible) absorption, transmission, and reflectance spectra of particles were acquired in an UV-Vis spectrophotometer (Model: U3600P) with an integrating sphere using $BaSO_4$ as a standard reference. Photoluminescence excitation and emission spectra were obtained using two spectrometers (Omni-λ3007 and Omni-λ180D; Zolix, Beijing, China) and a 150 W Xenon lamp as the excitation source. The Commission International de I'Eclairage (CIE) chromaticity coordinates of sample were calculated by CIE 1931 software (V.1.6.0.2). Magnetic properties were collected on a Quantum Design superconducting quantum interference device (SQUID) magnetometer (MPMS XL-7).

3. Results and Discussion

Figure 1 shows the typical XRD patterns of the Tb^{3+} doped Na_3FeF_6 samples synthesized with different doping concentrations of Tb^{3+} (5%, 10%, 15%, 18%, and 20%). The diffraction peaks of all samples clearly match that of the standard pattern of Na_3AlF_6 (JCPDS no. 12-0907), indicating the structure of obtained samples is isomorphic with cryolite-like structures (Na_3AlF_6 and Na_3CrF_6) that belongs to the space group P21/c [24–26]. This result agrees with previous report about the structure of Na_3FeF_6 [27]. The three-dimensional crystal structure of Na_3FeF_6:Tb^{3+} is shown in Figure 2. There are three different sodium sites, namely Na1, Na2, and Na3, as highlighted in Figure 2b. Na1 site is located at the distorted octahedral site of (NaF_6), Na2 site is located at the bi-pyramid site of (NaF_5), and the Na3 site is located at the distorted tetrahedral site of (NaF_4). As can be observed from the crystal structure (Figure 2a), Na1 octahedral and Na3 tetrahedral share corners. Na1 octahedral share

edges with Na2 bipyramid. Furthermore, all Fe atoms are located at the distorted FeF_6 octahedral sites. FeF_6 octahedra share corners with Na1 octahedral and Na3 tetrahedral share edges with Na2 bi-pyramid. In this structure, Fe^{3+} sites can be taken by Tb^{3+} ions in Tb doped Na_3FeF_6. According to the Bragg equation ($2dSin\theta = n\lambda$), d increases with the decreasing of θ. Figure 1 shows that diffraction peak of Na_3FeF_6:Tb^{3+} is all shifted to the left compared with that of Na_3AlF_6 due to the larger ionic size of Fe^{3+} as compared with that of Al^{3+}. As concentration of the Tb ions increases from 5% to 18%, the diffraction peak gradually shifts to the left, diffraction angle θ decreases. This result can be explained by the substitution of Fe^{3+} (ionic radius = 0.65 Å) [28] by Tb^{3+} with a larger ionic radius (0.92 Å) [29]. Therefore, the lattice constant would increase with the increase in the concentration of Tb ions in the lattice. The diffraction peaks of the Na_3FeF_6 with 18% Tb^{3+} doping are the highest, indicating the best crystallinity. The increase of Tb^{3+} concentration above 18% leads to growth of lattice strain that prevents the further enhancement of crystallization. To further confirm the ions of Tb^{3+} is present in the form of Tb-F and Na_3FeF_6:18%Tb^{3+} powder was analyzed by XPS (Figure S1). The XPS spectrum shows the presence of Na, F, Fe and Tb elements. Figure S1b shown the XPS spectra of Tb(Ds-4s), Na(2p), F(2s), Fe(3p), Tb(4d) from Na_3FeF_6:18%Tb^{3+} and the relatively strong peaks at around 7.5, 152 eV can be assigned to the binding energy of Tb (Ds-4s) and Tb (4d), respectively. The peak around 24.7 eV is attributed to the binding energy of Na(2p). The binding energy of F(2s) around 30.3 eV and F(1s) around 684.9 eV are found in spectra of XPS (Figure 1b,d). The Fe(3p) peaks show a doublet around 56.3 and 59.1 eV, corresponding to structure of FeF_3 and FeF_2, respectively. The result in accordance with the discussion of the XRD patterns of the Tb^{3+} doped Na_3FeF_6.

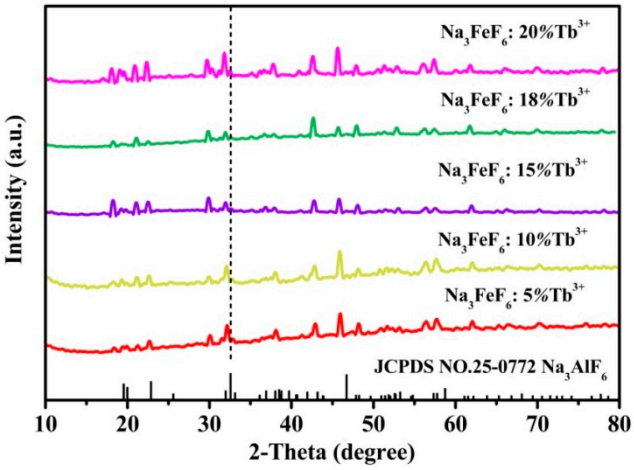

Figure 1. X-ray diffraction (XRD) patterns for samples of the Na_3FeF_6:Tb^{3+} with different Tb^{3+}-doping concentrations.

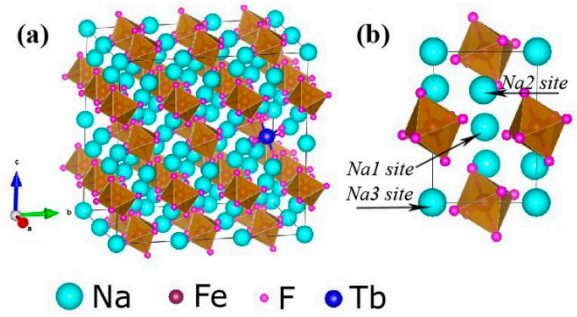

Figure 2. (**a**) Three-dimensional crystal structure of Na_3FeF_6:Tb^{3+}. (**b**) Three different sodium sites in the Na_3FeF_6 crystal structure.

The Na_3FeF_6:18%Tb^{3+} particles are then observed by FESEM equipped with an energy dispersive spectroscopy (EDS) device. Figure 3a–c show the FESEM images with low magnification (a) and

high magnification (b,c). It can be observed from Figure 3a that the as-prepared samples consist of randomly distributed octahedral particles with a relatively uniform size and shape (edge lengths are approximately 10 μm). As the magnification increases (Figure 3c), it can be seen clearly that the surfaces of the octahedron are almost smooth, but covered by a few small sized particles. EDS analysis was then used to determine the distribution of elements, as illustrated in Figure 3c. The results confirm the dominance of four elements:F, Fe, Na and Tb. In addition, the corresponding EDS mapping images given in Figure 3d–g reveal that all the elements are distribute homogeneously in the particles and Tb ions are successfully doped into the lattice of Na_3FeF_6.

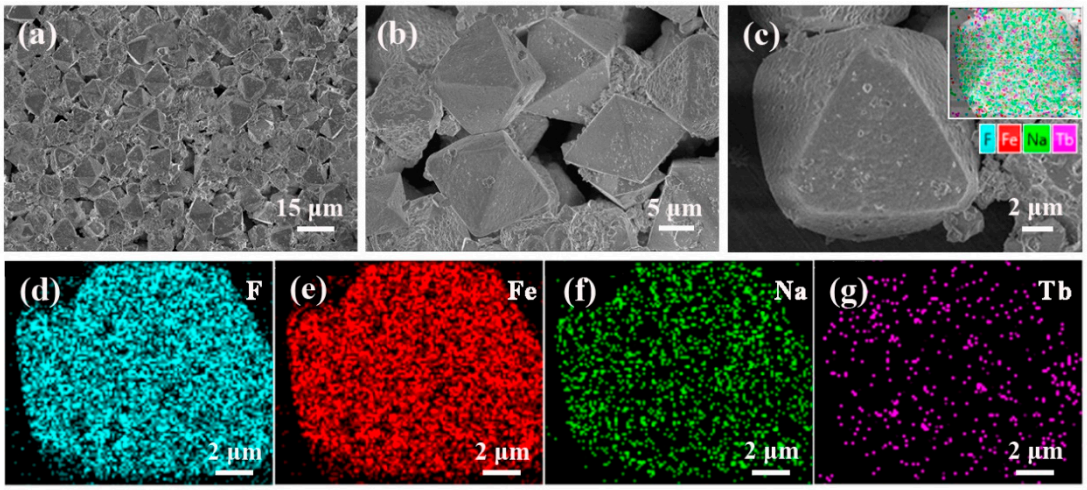

Figure 3. (**a**–**c**) Field emission scanning electron microscopy (FESEM) images of the Na_3FeF_6:18%Tb^{3+} powders and (**d**–**g**) the corresponding energy dispersive spectroscopy (EDS) mapping for elements image F, Fe, Na, and Tb.

To confirm the optical response of the particles in the UV-Vis range, absorption spectra was detected by an UV-Vis spectrophotometer. As shown in Figure 4, all samples exhibit obvious ultraviolet absorption at wavelength short than 300 nm, which can be attributed to transition of the 4f electronic ground state to the 5d energy levels, namely $^4f_8 \rightarrow {}^4f_7{}^5d_1$ energy levels transitions of Tb^{3+} [30]. The f-f transitions of the Tb^{3+} in the wavelength region of 300-400 nm are relatively weak and these peaks at 355 and 380 nm by f-f transitions of Tb^{3+} are almost invisible in the absorption spectra [31]. The transmission spectra and the reflectance spectra of the Na_3FeF_6:18%Tb^{3+} particles correspond to the absorption spectra (as shown in Figure S2).

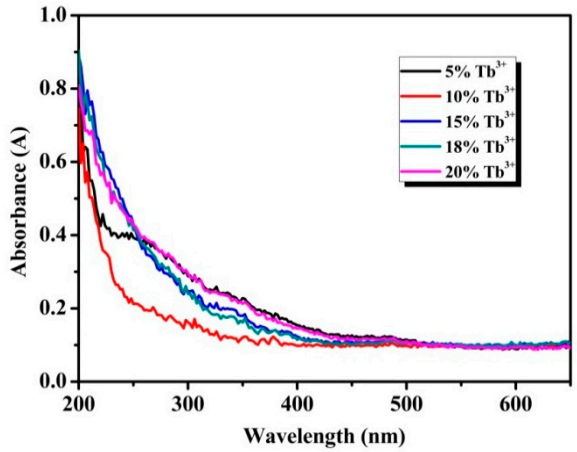

Figure 4. Ultraviolet-visible (UV-Vis) absorption spectra of Na_3FeF_6:Tb^{3+} particles with different Tb^{3+}-doping concentrations.

In order to further study the optical properties of the Na_3FeF_6:Tb^{3+} particles, excitation and emission spectra are measured by fluorescence spectrometers. Figure 5 presents the excitation and emission spectra, and CIE 1931 chromaticity coordinates of the samples together with the energy level diagram of Tb ions. As shown in Figure 5a, the excitation spectra of Na_3FeF_6:18%Tb^{3+} are measured for the emission wavelength of 592 nm. It can be observed that the excitation spectra consist of sharp and intense bands with peak positions at 355 and 375 nm along with weak bands at 280 and 320 nm, which can be assigned to the $^7F_6 \rightarrow {}^5L_{10}$, $^7F_6 \rightarrow {}^5G_6$, $^7F_6 \rightarrow {}^3H_6$ and $^7F_6 \rightarrow {}^5D_1$ transitions of the Tb^{3+}, respectively [32–34].

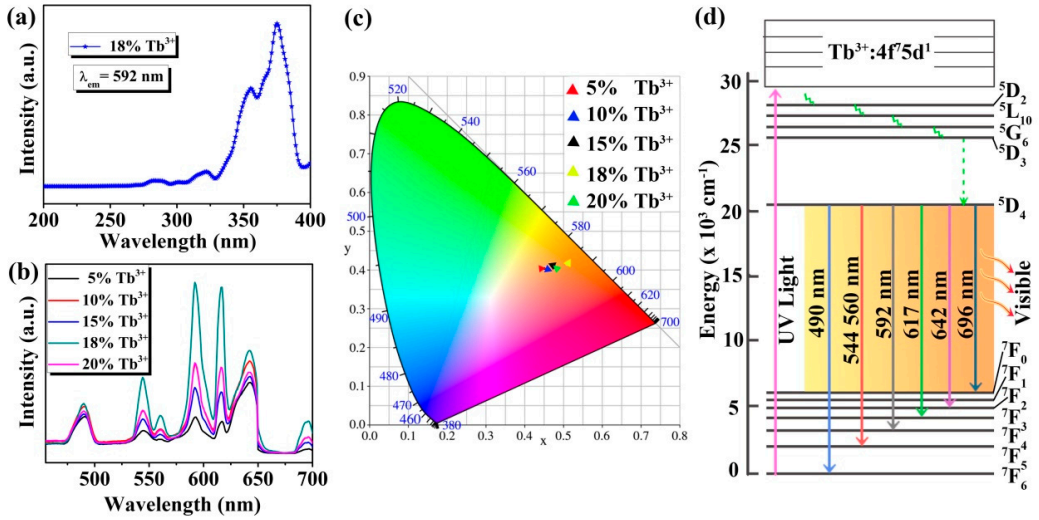

Figure 5. (**a**) Excitation spectrum of Na_3FeF_6:18%Tb^{3+}; (**b**) emission spectra of Na_3FeF_6:Tb^{3+} particles with different Tb^{3+}-doping concentrations; (**c**) CIE 1931 chromaticity diagram of Na_3FeF_6 doped with different concentration of Tb^{3+}; (**d**) simplified energy levels diagram of the Tb ions.

Since the peak of 375 nm is the strongest in the excitation spectrum, the emission spectra are recorded at this excitation wavelength for Na_3FeF_6:Tb^{3+} particles with different Tb^{3+}-doping concentrations. As can be seen from Figure 5b, the emission spectra in the region of 455–700 nm exhibit seven peaks at 490, 544, 560, 592, 617, 642, and 696 nm due to $^5D_4 \rightarrow {}^7F_6$, $^7F_5$, $^7F_5$, $^7F_4$, $^7F_3$, $^7F_2$ and $^7F_0$ transitions, respectively [35–38]. Among the seven peaks, five peaks at 490, 544, 592, 617, and 642 nm are much stronger, while the other two peaks (560 and 696 nm) are relatively weak. In addition, among the five samples, the luminescence intensity is strongest when the doping concentration of Tb^{3+} is 18%, and the highest luminescence peak is at 592 nm. The emission spectrum is converted to the CIE 1931 chromaticity coordinates using the photoluminescence data to better characterize the emission color of the samples. From the CIE 1931 chromaticity diagram (Figure 5c), it is found that all samples emit orange-red light, which is different from the traditional green light emission of Tb^{3+} ions. This may be due to the use of a new host (Na_3FeF_6) which favors the emission in the longer wavelengths. Furthermore, Figure 5c shows that as the doping concentration of Tb ions increases, the luminescence intensity first increases and then decreases, and the luminescence is strongest at the doping concentration of 18%, which is consistent with the emission spectrum (Figure 5b). The CIE coordinates of Na_3FeF_6:18%Tb^{3+} are X = 0.5103 and Y = 0.4155, which show a typical orange-red color.

In order to better understand the luminescence mechanism of the samples, we combined the energy level diagram of Tb ions (Figure 5d) and take the luminescence at 592 nm as an example to explain the involved electronic transitions. Upon excitation by ultraviolet light (UV-light), Tb^{3+} ions are promoted from the ground state ($^7F_6$) to the excited state (for example $^5L_{10}$, $^5G_6$). Subsequently, the level $^5D_4$ of Tb^{3+} ions is populated by radiation-free transition. Finally, the Tb^{3+} ions relax to the ground state ($^7F_4$) by giving visible emission at around 592 nm. The visible luminescence at other wavelengths is similar to the emission at 592 nm.

Figure 6a shows the temperature-dependence magnetization plots (M-T) in a temperature range between 5 K and 300 K in a 2000 Oe field of Na_3FeF_6:Tb^{3+} particles. It is found that the magnetization decreases rapidly from about 24.74 emu/g at 5 K to 1.06 emu/g at 50 K, and then slowly decreases with a temperature increase from 50 K to 300 K, typical for paramagnetic materials. The magnetization versus magnetic field (M-H) curves at 300 K of Na_3FeF_6:18%Tb^{3+} particles obtained by SQUID magnetometry are presented in Figure 6b. As the strength of the applied magnetic field increasing, the ideal linear correlation between the magnetization and the applied magnetic field was obtained, indicating that Na_3FeF_6:Tb^{3+} possesses paramagnetism. The results show that the synthesized samples might be used as magneto-optical bifunctional materials.

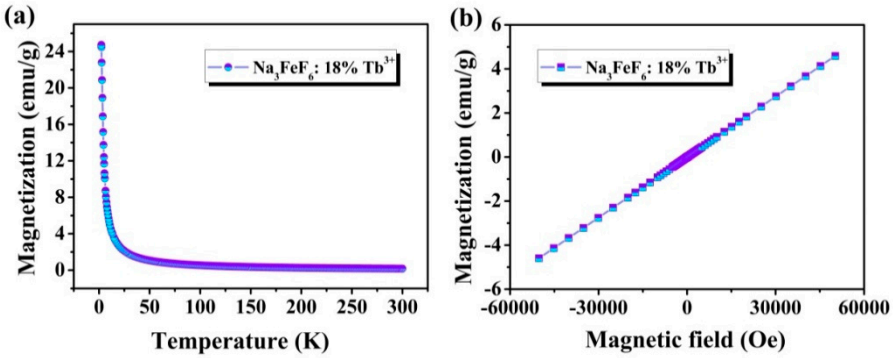

Figure 6. (**a**) Temperature-dependent magnetization (M-T) curves measured at 2000 Oe for Na_3FeF_6:18%Tb^{3+} particles; (**b**) magnetization versus magnetic field (M-H) curve at 300 K of Na_3FeF_6:18%Tb^{3+} particles.

4. Conclusions

In summary, monodispersed Na_3FeF_6:Tb^{3+} octahedral particles have been successfully synthesized by a facile one-pot hydrothermal process and the results of XRD and SEM indicated that Na_3FeF_6:Tb^{3+} octahedral belong to a monoclinic crystal structure (space group P21/c). The Na_3FeF_6:Tb^{3+} octahedral particles emit orange-red colored light attributed to the $^5D_4 \rightarrow {}^7F_J$ transitions of the Tb^{3+} ions. The luminescence intensity of the Na_3FeF_6:Tb^{3+} reaches maximum at Tb^{3+} doping concentration of 18%. The M-T and M-H curves confirm that Na_3FeF_6:Tb^{3+} particles are paramagnetic with a high magnetic moment. These results indicate that the obtained Na_3FeF_6:Tb^{3+} octahedral particles might be used as a magnetic-optical bi-functional material for various potential applications in biomedical fields and magneto-optical modulation.

Supplementary Materials: The following are available online at http://www.mdpi.com/1996-1944/13/2/320/s1.

Author Contributions: Z.Z. conceptualization, methodology, data curation and writing-original draft preparation; X.L. preparation of sample, supervision of the work, editing, and review of the manuscript. All authors have read and agreed to the published version of the manuscript.

Funding: This work was financially supported by the National Natural Science Foundation of China (Grant Nos. 61575091, 61675094, and 51471082), excellent Team of Spectrum Technology and Application of Henan province (Grant No. 18024123007).

Conflicts of Interest: The authors declare no conflict of interest.

References

1. Gai, S.; Yang, P.; Li, C.; Wang, W.; Dai, Y.; Niu, N.; Lin, J. Synthesis of Magnetic, Up-Conversion Luminescent, and Mesoporous Core-Shell-Structured Nanocomposites as Drug Carriers. *Adv. Funct. Mater.* **2010**, *20*, 1166–1172. [CrossRef]
2. Xiao, Q.; Zhang, Y.; Zhang, H.; Dong, G.; Han, J.; Qiu, J. Dynamically tuning the up-conversion luminescence of Er^{3+}/Yb^{3+} co-doped sodium niobate nano-crystals through magnetic field. *Sci. Rep.* **2016**, *6*, 31327. [CrossRef] [PubMed]

3. Huang, C.C.; Su, C.H.; Liao, M.Y.; Yeh, C.S. Magneto-optical $FeGa_2O_4$ nanoparticles as dual-modality high contrast efficacy T-2 imaging and cathodoluminescent agents. *PCCP* **2009**, *11*, 6331–6334. [CrossRef] [PubMed]
4. Huang, C.C.; Liu, T.Y.; Su, C.H.; Lo, Y.W.; Chen, J.H.; Yeh, C.S. Superparamagnetic hollow and paramagnetic porous Gd_2O_3 particles. *Chem. Mater.* **2008**, *20*, 3840–3848. [CrossRef]
5. Jung, H.K.; Kim, C.H.; Hong, A.R.; Lee, S.H.; Kim, T.C.; Jang, H.S.; Kim, D.H. Luminescent and magnetic properties of cerium-doped yttrium aluminum garnet and yttrium iron garnet composites. *Ceram. Int.* **2019**, *45*, 9846–9851. [CrossRef]
6. Chen, H.; Qi, B.; Moore, T.; Colvin, D.C.; Crawford, T.; Gore, J.C.; Alexis, F.; Mefford, O.T.; Anker, J.N. Synthesis of brightly PEGylated luminescent magnetic upconversion nanophosphors for deep tissue and dual MRI imaging. *Small* **2014**, *10*, 160–168. [CrossRef]
7. Hu, Q.; Jia, Z.; Yin, Y.; Mu, W.; Zhang, J.; Tao, X. Crystal growth, thermal and optical properties of TSLAG magneto-optical crystals. *J. Alloys Compd.* **2019**, *805*, 496–501. [CrossRef]
8. Li, J.; Tang, T.; Luo, L.; Li, N.; Zhang, P. Spin Hall effect of reflected light in dielectric magneto-optical thin film with a double-negative metamaterial substrate. *Opt. Express* **2017**, *25*, 19117–19128. [CrossRef]
9. Yang, M.; Zhou, D.; Xu, J.; Tian, T.; Jia, R.; Wang, Z. Fabrication and magneto-optical property of yttria stabilized Tb_2O_3 transparent ceramics. *J. Eur. Ceram. Soc.* **2019**, *39*, 5005–5009. [CrossRef]
10. Ye, S.; Zhang, Y.; He, H.; Qiu, J.; Dong, G. Simultaneous broadband near-infrared emission and magnetic properties of single phase Ni^{2+}-doped β-Ga_2O_3 nanocrystals via mediated phase-controlled synthesis. *J. Mater. Chem. C* **2015**, *3*, 2886–2896. [CrossRef]
11. Zhang, Y.; Xiao, Q.; He, H.; Zhang, J.; Dong, G.; Han, J.; Qiu, J. Simultaneous luminescence modulation and magnetic field detection via magneto-optical response of Eu^{3+}-doped $NaGdF_4$ nanocrystals. *J. Mater. Chem. C* **2015**, *3*, 10140–10145. [CrossRef]
12. Gu, H.; Zheng, R.; Zhang, X.; Xu, B. Facile one-pot synthesis of bifunctional heterodimers of nanoparticles: A conjugate of quantum dot and magnetic nanoparticles. *J. Am. Chem. Soc.* **2004**, *126*, 5664–5665. [CrossRef] [PubMed]
13. Zhang, F.; Braun, G.B.; Pallaoro, A.; Zhang, Y.; Shi, Y.; Cui, D.; Moskovits, M.; Zhao, D.; Stucky, G.D. Mesoporous multifunctional upconversion luminescent and magnetic "nanorattle" materials for targeted chemotherapy. *Nano Lett.* **2011**, *12*, 61–67. [CrossRef] [PubMed]
14. Jia, H.; Zhou, Y.; Li, X.; Li, Y.; Zhang, W.; Fu, H.; Zhao, J.; Pan, L.; Liu, X.; Qiu, J. Synthesis and phase transformation of $NaGdF_4$: Yb–Er thin films using electro-deposition method at moderate temperatures. *CrystEngComm* **2018**, *20*, 6919–6924. [CrossRef]
15. Jia, H.; Liu, Z.; Liao, L.; Gu, Y.; Ding, C.; Zhao, J.; Zhang, W.; Hu, X.; Feng, X.; Chen, Z. Upconversion Luminescence from Ln^{3+} (Ho^{3+}, Pr^{3+}) Ion-Doped $BaCl_2$ Particles via NIR Light of Sun Excitation. *J. Phys. Chem. C* **2018**, *122*, 9606–9610. [CrossRef]
16. Tan, C.; Ma, B.; Zhang, J.; Zuo, Y.; Zhu, W.; Liu, Y.; Li, W.; Zhang, Y. Pure red upconversion photoluminescence and paramagnetic properties of Gd_2O_3: Yb^{3+}, Er^{3+} nanotubes prepared via a facile hydrothermal process. *Mater. Lett.* **2012**, *73*, 147–149. [CrossRef]
17. Zhang, L.; Yin, M.; You, H.; Yang, M.; Song, Y.; Huang, Y. Mutifuntional $GdPO_4$: Eu^{3+} hollow spheres: Synthesis and magnetic and luminescent properties. *Inorg. Chem.* **2011**, *50*, 10608–10613. [CrossRef]
18. Ma, Z.W.; Zhang, J.P.; Wang, X.; Yu, Y.; Han, J.B.; Du, G.H.; Li, L. Magnetic field induced great photoluminescence enhancement in an Er^{3+}: YVO_4 single crystal used for high magnetic field calibration. *Opt. Lett.* **2013**, *38*, 3754–3757. [CrossRef]
19. Zhu, X.; Tu, H.; Hu, Z.; Zhuang, N. Enhancement of magneto-optical performance of $Tb_{0.94}Pr_{0.06}VO_4$ single crystals by Pr doping. *Mater. Lett.* **2019**, *242*, 195–198. [CrossRef]
20. Chen, P.; Zhong, Z.; Jia, H.; Zhou, J.; Han, J.; Liu, X.; Qiu, J. Magnetic field enhanced upconversion luminescence and magnetic-optical hysteresis behaviors in $NaYF_4$: Yb, Ho nanoparticles. *RSC Adv.* **2016**, *6*, 7391–7395. [CrossRef]
21. Zhang, L.; Wang, Y.S.; Yang, Y.; Zhang, F.; Dong, W.F.; Zhou, S.Y.; Pei, W.H.; Chen, H.D.; Sun, H.B. Magnetic/upconversion luminescent mesoparticles of Fe_3O_4@ LaF_3: Yb^{3+}, Er^{3+} for dual-modal bioimaging. *Chem. Commun.* **2012**, *48*, 11238–11240. [CrossRef] [PubMed]

22. Peng, H.; Cui, B.; Li, G.; Wang, Y.; Li, N.; Chang, Z.; Wang, Y. A multifunctional β-CD-modified Fe_3O_4@ ZnO: Er^{3+}, Yb^{3+} nanocarrier for antitumor drug delivery and microwave-triggered drug release. *Mater. Sci. Eng. C* **2015**, *46*, 253–263. [CrossRef] [PubMed]
23. Zhang, Y.; Pan, S.; Teng, X.; Luo, Y.; Li, G. Bifunctional magnetic- luminescent nanocomposites: Y_2O_3/Tb nanorods on the surface of iron oxide/silica core-shell nanostructures. *J. Phys. Chem. C* **2008**, *112*, 9623–9626. [CrossRef]
24. Brunton, G. The crystal structure of Na_3CrF_6. *Mater. Res. Bull.* **1969**, *4*, 621–626. [CrossRef]
25. Shakoor, R.A.; Lim, S.Y.; Kim, H.; Nam, K.W.; Kang, J.K.; Kang, K.; Choi, J.W. Mechanochemical synthesis and electrochemical behavior of Na_3FeF_6 in sodium and lithium batteries. *Solid State Ion.* **2012**, *218*, 35–40. [CrossRef]
26. Chen, J.Y.; Lin, C.W.; Lin, P.H.; Li, C.W.; Liang, Y.M.; Liu, J.C.; Chen, S.S. Fluoride recovery from spent fluoride etching solution through crystallization of Na_3AlF_6 (synthetic cryolite). *Sep. Purif. Technol.* **2014**, *137*, 53–58. [CrossRef]
27. Jia, H.; Zhou, Y.; Wang, X.; Zhang, W.; Feng, X.; Li, Z.; Fu, H.; Zhao, J.; Liu, Z.; Liu, X. Luminescent properties of Eu-doped magnetic Na_3FeF_6. *RSC Adv.* **2018**, *8*, 38410–38415. [CrossRef]
28. Pang, Y.L.; Abdullah, A.Z. Effect of low Fe^{3+} doping on characteristics, sonocatalytic activity and reusability of TiO_2 nanotubes catalysts for removal of Rhodamine B from water. *J. Hazard. Mater.* **2012**, *235*, 326–335. [CrossRef]
29. Li, X.; Dong, M.; Hu, F.; Qin, Y.; Zhao, L.; Wei, X.; Chen, Y.; Duan, C.; Yin, M. Efficient sensitization of Tb^{3+} emission by Dy^{3+} in $CaMoO_4$ phosphors: Energy transfer, tunable emission and optical thermometry. *Ceram. Int.* **2016**, *42*, 6094–6099. [CrossRef]
30. Bi, F.; Dong, X.; Wang, J.; Liu, G. Electrospinning preparation and photoluminescence properties of $Y_3Al_5O_{12}$: Tb^{3+} nanostructures. *Luminescence* **2015**, *30*, 751–759. [CrossRef]
31. Singh, V.; Singh, N.; Pathak, M.S.; Singh, P.K.; Natarajan, V. Tb^{3+} doped Ca_2La_8 (SiO_4) $_6O_2$ oxyapatite phosphors. *Optik* **2018**, *171*, 356–362. [CrossRef]
32. Kumar, J.S.; Pavani, K.; Sasikala, T.; Jayasimhadri, M.; Jang, K.; Moorthy, L.R. Concentration dependent luminescence characteristics of $^5D_4$ and $^5D_3$ excited states of Tb^{3+} ions in CFB glasses. *Proc. SPIE* **2011**, 79401H. [CrossRef]
33. Cho, I.; Kang, J.G.; Sohn, Y. Photoluminescence imaging of SiO_2@ Y_2O_3: Eu (III) and SiO_2@ Y_2O_3: Tb (III) core-shell nanostructures. *Bull. Korean Chem. Soc.* **2014**, *35*, 575–580. [CrossRef]
34. Wang, D.Y.; Chen, Y.C.; Huang, C.H.; Cheng, B.M.; Chen, T.M. Photoluminescence investigations on a novel green-emitting phosphor Ba_3Sc $(BO_3)_3$: Tb^{3+} using synchrotron vacuum ultraviolet radiation. *J. Mater. Chem.* **2012**, *22*, 9957–9962. [CrossRef]
35. Van Do, P.; Quang, V.X.; Thanh, L.D.; Tuyen, V.P.; Ca, N.X.; Hoa, V.X.; Van Tuyen, H. Energy transfer and white light emission of $KGdF_4$ polycrystalline co-doped with Tb^{3+}/Sm^{3+} ions. *Opt. Mater.* **2019**, *92*, 174–180. [CrossRef]
36. Shi, J.; Wang, Y.; Huang, L.; Lu, P.; Sun, Q.; Wang, Y.; Tang, J.; Belfiore, L.A.; Kipper, M.J. Polyvinylpyrrolidone nanofibers encapsulating an anhydrous preparation of fluorescent SiO_2-Tb^{3+} nanoparticles. *Nanomaterials* **2019**, *9*, 510. [CrossRef] [PubMed]
37. Blasse, G.; Bril, A. Investigations of Tb^{3+}-activated phosphors. *Philips Res. Rep.* **1967**, *22*, 481–504.
38. Scholl, M.S.; Trimmier, J.R. Luminescence of YAG: Tm, Tb. *J. Electrochem. Soc.* **1986**, *133*, 643–648. [CrossRef]